Universiteit
Leiden
The Netherlands

# Asymmetric block copolymers confined in a thin film

Huinink, H.P.; Brokken-Zijp, J.C.M.; Dijk, M.A. van; Sevink, G.J.A.

**Citation**
Huinink, H. P., Brokken-Zijp, J. C. M., Dijk, M. A. van, & Sevink, G. J. A. (2000). Asymmetric block copolymers confined in a thin film. *Journal Of Chemical Physics*, *112*(5), 2452-2462. doi:10.1063/1.480811

Version: Not Applicable (or Unknown)
License: Leiden University Non-exclusive license
Downloaded from: https://hdl.handle.net/1887/66559

**Note:** To cite this publication please use the final published version (if applicable).

# Asymmetric block copolymers confined in a thin film

H. P. Huinink, J. C. M. Brokken-Zijp, M. A. van Dijk, and G. J. A. Sevink

Citation: The Journal of Chemical Physics **112**, 2452 (2000); doi: 10.1063/1.480811
View online: https://doi.org/10.1063/1.480811
View Table of Contents: http://aip.scitation.org/toc/jcp/112/5
Published by the American Institute of Physics

**Articles you may be interested in**

Thin films of block copolymer
The Journal of Chemical Physics **106**, 7781 (1997); 10.1063/1.473778

Block Copolymers—Designer Soft Materials
Physics Today **52**, 32 (1999); 10.1063/1.882522

Phase behavior in thin films of cylinder-forming ABA block copolymers: Mesoscale modeling
The Journal of Chemical Physics **120**, 1117 (2004); 10.1063/1.1627325

Fluctuation effects in the theory of microphase separation in block copolymers
The Journal of Chemical Physics **87**, 697 (1987); 10.1063/1.453566

Phase behavior in thin films of cylinder-forming ABA block copolymers: Experiments
The Journal of Chemical Physics **120**, 1105 (2004); 10.1063/1.1627324

Block copolymer microstructures in the intermediate-segregation regime
The Journal of Chemical Physics **106**, 2436 (1997); 10.1063/1.473153

PHYSICS TODAY
WHITEPAPERS

ADVANCED LIGHT CURE ADHESIVES

Take a closer look at what these environmentally friendly adhesive systems can do

READ NOW

PRESENTED BY
MASTERBOND
ADHESIVES | SEALANTS | COATINGS

# Asymmetric block copolymers confined in a thin film

H. P. Huinink, J. C. M. Brokken-Zijp, and M. A. van Dijk[a)]
*Shell Research and Technology Centre Amsterdam, Badhuisweg 3, 1031 CM Amsterdam, The Netherlands*

G. J. A. Sevink
*Faculty of Mathematics and Natural Science, University of Groningen, Nijenborgh 4, 9747 AG Groningen, The Netherlands*

(Received 23 July 1999; accepted 26 October 1999)

We have used a dynamic density functional theory (DDFT) for polymeric systems, to simulate the formation of micro phases in a melt of an asymmetric block copolymer, $A_nB_m(f_A=1/3)$, both in the bulk and in a thin film. In the DDFT model a polymer is represented as a chain of springs and beads. A spring mimics the stretching behavior of a chain fragment and the spring constant is calculated with the Gaussian chain approximation. Simulations were always started from a homogeneous system. We have mainly investigated the final morphology, adopted by the system. First, we have studied the bulk behavior. The diblock copolymer forms a hexagonal packed array of *A*-rich cylinders, embedded in a *B*-rich matrix. Film calculations have been done by confining a polymer melt in a slit. Both the slit width and surface-polymer interactions were varied. With the outcomes a phase diagram for confined films has been constructed. Various phases are predicted: parallel cylinders ($C_{\parallel}$), perpendicular cylinders ($C_{\perp}$), parallel lamellae ($L_{\parallel}$), and parallel perforated lamellae ($CL_{\parallel}$). When the film surfaces are preferentially wet by either the *A* or the *B* block, parallel oriented microdomains are preferred. A perpendicular cylindrical phase is stable when neither the *A* nor *B* block preferentially wets the surfaces. The predicted phase diagram is in accordance with experimental data in the literature and explains the experimentally observed differences between films of asymmetric block copolymers with only two parameters: the film thickness and the energetic preference of the surface for one of the polymer blocks. We have also observed, that confinement speeds up the process of long range ordering of the microdomains. © *2000 American Institute of Physics.* [S0021-9606(00)70504-6]

## I. INTRODUCTION

### A. Block copolymer thin films

The physics behind the microstructure of block copolymer materials has been investigated extensively in the last three decades. From a scientific point of view, these materials are interesting, because order–disorder transitions can be studied under relatively simple experimental conditions and a variety of microstructures have been observed.[1,2] Various types of block copolymers are also commercially interesting because they are able to improve the mechanical properties of materials. Typical examples of copolymers of industrial interest are polystyrene-polybutadiene (PS–PB or PS–PB–PS) block copolymers, widely applied in bitumen for roofing and road application, in adhesives and in a range of polymeric materials.

The last decade also a growing amount of studies on films of block copolymers have been published in the literature.[3,4] The most important objective for these studies seems to be the search for surfaces with controllable patterns on a nanometer scale, which could be useful in electronic applications.

Up until now, most of the work has been done on symmetric diblock copolymers, $f\approx 0.5$. Thin films have been studied extensively by experiments[5–15] and theory.[16–21] In these films the microdomains have a lamellar shape as in a bulk system. The lamellae align parallel with the film, when a difference between the surface energies of the two blocks exists (selective interfaces). In unconfined films, terraces are formed with a step height of about the equilibrium lamellar period in the bulk, because the thickness of a homogeneous film is not commensurate with an integer amount of lamellae without frustrating the lamellar period.[6,7,18,19,20] In confined films, frustration cannot be avoided and the lamellar period deviates from the bulk value.[13,16] Random copolymers have been used to tune the interactions between the interfaces and the two different copolymer blocks.[14,15] Films with nonselective surfaces have been prepared in this way. In these films, confined and unconfined, the frustration of the lamellar period is avoided by changing the orientation of the lamellae from parallel with to perpendicular to the film surfaces.

Relatively little work has been done on films of asymmetric block copolymers. It is hard to sketch a complete picture of the film behavior with the help of the experimental data[22–31] and theoretical investigations,[32,33] published in the literature. Our research will focus on block copolymers, that form cylindrical domains in the bulk melt. All experimental studies seem to agree that parallel aligned cylinders are present in equilibrated films with a thickness larger then a few domains ($>2D$). A perpendicular oriented cylindrical phase has been observed, but it was shown that this morphol-

a)Author to whom correspondence should be addressed. Electronic mail: Menno.A.vanDijk@opc.shell.com

 © 2000 American Institute of Physics

ogy was caused by rapid solvent evaporation during the film preparation.[30] Various observations have been made for thin films ($<2D$). In example, it is thought that perpendicular oriented cylinders are formed in unconfined films of PS–PB–PS (30% S) supported by a solid substrate,[25] channel-like structures have been observed in free standing films of PS–PB (30% S) (Refs. 28, 31) and other noncylindrical morphologies, have been observed too.[23,24,28] The presence of noncylindrical morphologies is an interesting feature of films of asymmetric copolymers. These observations support a weak segregation limit (WSL) analysis, which has predicted that homogeneous surface fields can drive a transition from a cylindrical to a lamellar phase.[32]

### B. This study

In this paper, we want to discuss model calculations on thin films of asymmetric diblock copolymers, that form a cylindrical phase in the bulk. We will systematically investigate the influences of both the film thickness and the surface interactions on the microstructure of the films.

Recently, new techniques have been developed to simulate the behavior of block copolymeric systems on mesoscopic length scales, i.e., dissipative particle dynamics (DPD) (Ref. 34) and a dynamic density functional theory (DDFT).[35] We have used the DDFT approach. The DDFT model combines the Langevin equation, which handles the dynamics on a mesoscopic scale, and a free energy functional for polymers, based on the Gaussian chain model. The model has previously been used to study the diffusive dynamics of the domain formation process of a symmetric diblock copolymer.[35,44] A detailed validation has been carried out on $(PO)_n(EO)_m(PO)_n$ block copolymer surfactants.[36] The theory was adapted to describe the behavior of block copolymer under shear.[37] Recently, the theory has been extended to study the influence of hard objects on the domain formation process of block copolymers.[38]

In fact, our study is a systematic investigation of a block copolymer melt in contact with a specific class of hard objects: infinite parallel surfaces. In our calculations we mimic a film as a polymer melt confined in a slit and assume that the finite size of the polymer/air interface can be neglected. We will construct a phase diagram, which will be compared with experimental data, reported in the literature. Although, we will focus on the final micro structure in the system, we will also briefly discuss the influence of confinement on the dynamics of domain formation process.

In this article, we will subsequently explain the most important features of the theoretical background of the used DDFT approach, give the parameters we have used in our calculations, discuss the results we have obtained, and draw conclusions.

## II. THEORY

### A. Dynamics

In the following sections we give a quick overview of the most important aspects of the DDFT model.[35,36,38,39] In the DDFT model a box with periodic boundaries is filled with fixed amounts of beads of different types, $\{N_I\}$. A polymer is represented as a string of beads. The core of the theory is the Langevin equation of motion, which describes the evolution of mesoscopic fields,[40] in our case the bead densities,

$$\frac{\partial \rho_I(\mathbf{r})}{\partial t} = M_I \nabla \cdot \rho_I(\mathbf{r}) \nabla \mu_I(\mathbf{r}) + \eta_I(\mathbf{r},t), \tag{1}$$

where $\rho_I(\mathbf{r})$, $M_I$, and $\mu_I(\mathbf{r})$ are the bead density field, the mobility parameter, and the intrinsic chemical potential field of a bead of type I, respectively. In principle, this equation is an extension of the diffusion equation. The last term on the right-hand side of Eq. (1) is stochastic noise, $\eta_I(\mathbf{r},t)$, which is distributed according to the fluctuation-dissipation theorem.[41]

As mentioned in the Introduction, we model a film as a polymer melt confined in a slit. Obviously, the surfaces of the slit are regarded as hard objects and mass transport through these objects has to be forbidden. Therefore, rigid-wall boundary conditions are used for the diffusion fluxes in the vicinity of the surfaces, $\nabla \mu_I \cdot \mathbf{n} = 0$, where $\mathbf{n}$ is the normal of the slit surface.

The two terms on the r.h.s. of Eq. (1) reflect the two origins of mass flux in the system. Diffusion fluxes are driven by variations of the bead chemical potential throughout the system. These fluxes will drive the system to states, which correspond to global or local minima of the free energy. Random fluxes are induced by the noise term. These random fluxes enable the system to overcome small energetic barriers. Without the noise, an unstable homogeneous mixture of molecules will not start to phase separate, because there is no driving force, $\nabla \mu_I(\mathbf{r}) = 0$.

### B. Free energy model

The field $\mu_I(\mathbf{r})$ connects the Langevin equation with the polymer model behind the DDFT formalism. This intrinsic chemical potential field can be calculated from the free energy, $F$, of the system, $\mu_I(\mathbf{r}) \equiv \delta F / \delta \rho_I(\mathbf{r})$. In the DDFT model the following free energy functional is used to model the behavior of an one-component polymer melt.[35,38]

$$\begin{aligned} F[\{\rho\}] = & -kT \ln \frac{\Phi''}{n!} - \sum_I \int_V U_I(\mathbf{r}) \rho_I(\mathbf{r}) d\mathbf{r} \\ & + \frac{1}{2} \sum_{I,J} \int_V \int_V \varepsilon_{IJ}(\mathbf{r}-\mathbf{r}') \rho_I(\mathbf{r}) \rho_J(\mathbf{r}') d\mathbf{r}' d\mathbf{r} \\ & + \frac{1}{2} \sum_I \int_V \int_V \varepsilon_{IM}(\mathbf{r}-\mathbf{r}') \rho_I(\mathbf{r}) \rho_M(\mathbf{r}') d\mathbf{r}' d\mathbf{r} \\ & + \frac{1}{2} \kappa_H v^2 \int_V \left( \sum_I \rho_I(\mathbf{r}) - \sum_I \overline{\rho_I} \right)^2 d\mathbf{r}, \end{aligned} \tag{2}$$

where $V$ is the system volume and $v$ is the excluded volume of a bead. Note that the excluded volumes of all bead types are chosen equal. The first two terms on the r.h.s. account for the entropy of a system of $n$ ideal Gaussian chains in an external field $U_I(\mathbf{r})$.[35] In the next section we will come back to these external fields. In Eq. (2) $\Phi$ is the single chain partition function. In the Gaussian approximation a polymer

chain is treated as a string of beads connected by springs with a spring constant of $3kT/2a^2$, where $a$ is the RMS end-to-end distance of the polymer chain fragment between two neighboring beads in the absence of external fields.[42]

The third term on the r.h.s. is the energy contribution of the bead–bead interactions. The bead–bead interaction potential $\varepsilon_{IJ}(\mathbf{r}-\mathbf{r}')$ has to describe the interactions between the chain fragments, captured by the beads $I$ and $J$ at the positions $\mathbf{r}$ and $\mathbf{r}'$. Gaussian kernels are used for these potentials,[35]

$$\varepsilon_{IJ}(\mathbf{r}-\mathbf{r}') \equiv \varepsilon_{IJ}^0 \left(\frac{3}{2\pi a^2}\right)^{3/2} \exp\left[-\frac{3}{2a^2}(\mathbf{r}-\mathbf{r}')^2\right]. \tag{3}$$

From Eq. (3) it follows that the range of the bead–bead interactions is comparable to the size of the chain fragments represented by the beads. The parameter $\varepsilon_{IJ}^0$ is related to the widely used Flory–Huggins parameter,[39] $\chi_{IJ}=(\varepsilon_{IJ}^0+\varepsilon_{JI}^0-\varepsilon_{II}^0-\varepsilon_{JJ}^0)/2\nu kT$, and can be interpreted as a cohesive energy. The functional form of the potential captures the most important physics of the interactions and is easy to handle in mathematical operations.

The fourth term of Eq. (2) models the interaction between the beads and the slit surfaces. The surface-bead potential has the same functional dependence as the bead–bead interaction potential (3). In the DDFT a density field $\rho_M(\mathbf{r})$ is assigned to the hard objects (masks); $\phi_M \equiv \rho_M \nu = 1$ inside and $\phi_M = 0$ outside the objects.[38]

The last term of Eq. (2) takes into account the excluded volume interactions, by imposing a free energy penalty when the total density deviates at a certain position from its average value.[39,43] The parameter $\kappa_H$ is the Helfand compressibility parameter.

### C. Density functionals: Dealing with hard surfaces

As said before, a polymer film is represented as a polymer melt confined between two parallel hard walls, a slit. In this section, we will shortly discuss how hard objects are incorporated in the DDFT approach.

In the preceding section, we have discussed the free energy model (2), but we did not address the external fields $U_I(\mathbf{r})$. These fields are conjugate with the density fields via the Gaussian chain density functional.[35] The distribution function of a single chain of $N$ beads with a certain conformation, given by a set of coordinates $\{\mathbf{r}_1,\ldots,\mathbf{r}_N\}$, is

$$\Psi(\mathbf{r}_1,\ldots,\mathbf{r}_N) = \frac{1}{\Phi}\exp\left[-\frac{3}{2a^2}\sum_{s=2}^{N}(\mathbf{r}_s-\mathbf{r}_{s-1})^2 - \sum_{s=1}^{N} U_s(\mathbf{r}_s)/kT\right]. \tag{4}$$

The first term in the exponent is the stretching entropy of an isolated Gaussian chain. The second term in the exponent, which contains the external field, incorporates the influence of the polymeric medium on the chain. The ensemble average bead density $\rho_s(\mathbf{r})$ of a certain bead $s$ at position $\mathbf{r}$ is as follows:[38]

$$\rho_s[U](\mathbf{r}) = c\mathcal{M}(\mathbf{r})\int_{\nu^N}\Psi(\mathbf{r}_1,\ldots,\mathbf{r}_N)\times\delta(\mathbf{r}-\mathbf{r}_s)d\mathbf{r}_1\cdots d\mathbf{r}_N, \tag{5}$$

where $C$ is a normalization constant[35] and $\mathcal{M}(\mathbf{r})$ is the so-called mask field, which defines the morphology of the hard objects in the system (in our case the slit surfaces). Inside a hard object $\mathcal{M}(\mathbf{r})=0(\phi_M=1)$ and outside $M(\mathbf{r})=1(\phi_M=0)$. Equation (5) can be evaluated efficiently with the help of a Green propagator formalism,[44] which we will not discuss in this article.

Due to the density functional (5), we have a closed set of equations. Using Eq. (5), the external fields $U_I(\mathbf{r})$ can be found given certain bead density profiles $\rho_I(\mathbf{r})$. When the fields $U_I(\mathbf{r})$ and $\rho_I(\mathbf{r})$ are known, the free energy $F$ can be calculated with Eq. (2). The chemical potential field $\mu_I(\mathbf{r})$ can be calculated from $F$. With $\mu_I(\mathbf{r})$ we are able to integrate the Langevin equation (1).

### D. Computational procedure

A Crank–Nicolson scheme is used for the numerical integration of Eq. (1).[35] Starting configurations for the integration are zero external potential fields and homogeneous density distributions. The time integration is carried out as long as the mesoscopic structure seems to change. The evolution of the density fields during the simulation is monitored with the help of an order parameter $P$, which is defined as follows:

$$P \equiv \frac{\nu^2}{V}\sum_I \int_{\mathbf{r}} (\rho_I^2(\mathbf{r}) - \overline{\rho_I^2}) d\mathbf{r}. \tag{6}$$

At $t=0$ $P$ equals zero. When the system has reached its equilibrium state or becomes trapped in a local minimum of the free energy, $P$ levels off to a constant value. When $P$ reaches a plateau value, the demixing of unlike beads is complete. However, this does not mean that the system is no longer in motion, because $P$ is insensitive to dynamic processes, that do not significantly increase the degree of demixing. Therefore, we use $P$ in combination with a direct evaluation of the density fields.

Even when no dynamics is observed in the density fields, we still have to be careful in stating that the system has reached a global or local minimum in the free energy, because it is possible that the time scales of the dynamics are beyond the time scale of our simulation.

### E. Confined and unconfined films

Many experiments on thin films, reported in the literature, are done with unconfined films. As a consequence, the film can form terraces in order to avoid unfavorable film thicknesses. In our calculations, we represent a film as a slit and therefore the layer is confined to a certain thickness and the terrace formation process can not be simulated directly. However, it is possible to predict the formation of terraces in unconfined films by analysing the free energy as a function of the slit width $H$.[21] If an uniform unconfined film with an area $A$ has an unfavorable thickness $H$, it can separate in two coexisting phases with thicknesses $H'$ and $H''$, which cover

the areas $A'$ and $A''$. The free energy of the unconfined film can be calculated form the free energy of a confined film, in our case the slit, with,

$$F_{\text{unconf}} = A' f_{\text{conf}}(H') + A'' f_{\text{conf}}(H''), \tag{7}$$

where $f_{\text{conf}}(H')$ is the free energy per unit area of the confined film with thickness $H'$. Minimization of Eq. (7) with respect to $H'$, $H''$, $A'$, and $A''$, given the constraints of conservation of film area, $A = A' + A''$, and material, $AH = A'H' + A''H''$, results in the following equalities;

$$\begin{aligned} \zeta &= \frac{\partial f_{\text{conf}}}{\partial H'} = \frac{\partial f_{\text{conf}}}{\partial H''}, \\ \zeta &= \frac{f_{\text{conf}}(H') - f_{\text{conf}}(H'')}{H' - H''}. \end{aligned} \tag{8}$$

The solution of these equalities can be obtained by plotting $f_{\text{conf}}$ as a function of $H$ and constructing a common tangent line.

## III. RESULTS AND DISCUSSION

### A. Parameters

All calculations are done with an $A_3B_6$ diblock copolymer model ($f \approx 0.33$). The number of beads in the polymer chain ($N = 9$) is small enough to ensure computational efficiency and large enough for a reasonable description of the configurational behavior of the chain.[36] The energetic interaction between beads of the same type is set to zero ($\varepsilon^0_{AA} = \varepsilon^0_{BB} = 0$). The $A-B$ interaction is chosen to be repulsive ($\varepsilon^0_{AB}/\nu kT = \chi = 2$). This parameter was obtained by fitting the order–disorder transition temperature of a PS–PB–PS triblock copolymer[45] with an $A_3B_{12}A_3$ model. As a consequence, the bulk behavior of this block copolymer is comparable with a SB block copolymer system with a $M_w \approx 35\,000$ g/mol at $T \approx 413$ K. We expect for this particular block copolymer system ($\chi N = 18$) a hexagonal packed cylindrical phase in the bulk.[46]

The calculations are done on a cubic grid, which has grid constant $h$. The bond length $a$ is chosen such that $a/h = 1.1543$, which is the optimal ratio for DDFT calculations.[44] The mobility parameters of the beads were assumed to be equal, $M_A = M_B = M$. The dimensionless time step is set to $\Delta\tau = M\Delta t/h^2 kT = 0.73$, which is larger then the optimal value 0.5 but small enough to ensure numerical stability. The noise scaling parameter is $\Omega = h^3/\nu = 100$ and the compressibility $\kappa_H/kT = 6$. It is known that this choice for $\Omega$ gives the best numerical performance for purely diffusive systems.[35,44] The chosen value for $\kappa_H$ is large enough to constrain the total density to the average total density and only allows small spatial fluctuations.

### B. Bulk behavior

Before we can discuss the domain formation of $A_3B_6$ in a slit, we have investigated its behavior in the bulk. We have simulated the micro phase separation process in a cubic box of dimension $L \times L \times L$ grid points ($L = 32$). The calculations were started with a homogeneous melt. In Fig. 1 we have plotted the order parameter $P$ as a function of time. In the interval $y \equiv \tau/\Delta\tau = [0,100]$, the separation of the $A$ and $B$ blocks into domains takes place. In this time span $A$- and $B$-rich domains are formed. In Fig. 2(a) the isodensity surfaces of the $A$ beads are shown, $\phi_A = \rho_A \nu = 0.33 (y = 100)$. The structure consists of a network of overlapping $A$-rich spheres embedded in a $B$-rich matrix. In the time interval $y = [100,1000]$ the separation of the $A$- and $B$-beads continues, the $A$-rich cylinders grow in length and a network is formed, Figs. 2(b) ($y = 200$) and 2(c) ($y = 1000$). At $y > 1000$, the network breaks down into separate cylinders, Fig. 2(d) ($y = 10\,000$). This last process clearly illustrates that the order parameter is not sensitive to all dynamics in the system. We can conclude that in a bulk system of $A_3B_6$ ($\chi N = 18$) a cylindrical phase is formed. However, they are still not packed in a hexagonal array. To observe hexagonal packing, a much longer simulation time should have been chosen, which was not useful for our purpose. The formation of a cylindrical phase is in agreement with self-consistent mean field (SCMF) calculations for $AB$ diblock copolymers.[46]

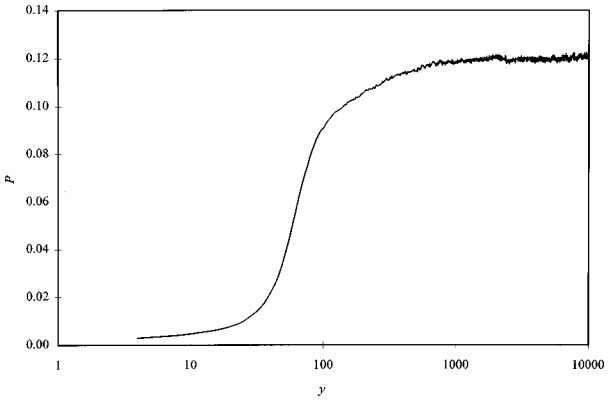


FIG. 1. The order parameter $P$ as a function of the number of time steps $y$ for a bulk system with the dimensions $32 \times 32 \times 32$.

To obtain the domain–domain distance of the $A_3B_6$ bulk system, $D_0$, we have also simulated in a $64 \times 64 \times 1$ box. Due to the assumption of homogeneity in one dimension, the development of long range order takes less time. After $y = 4000$ a reasonable hexagonal pattern has developed, Fig. 3. We have determined by hand that $D_0 = 7 \pm 0.5$.

### C. Phase behavior in a slit

The slit calculations have been performed in boxes of dimension $L \times L \times W$ grid points. All calculations have been done with $L = 32$, which is large enough to avoid strong boundary effects on the final microstructure and small enough to ensure a reasonable computational speed, needed to do a systematic analysis. The slit surfaces were represented as planes with a thickness of 1 grid point and positioned parallel to the $L \times L$ faces of the box. The two surfaces were placed at the box boundaries, see Fig. 4. The resulting slit width $H$ equals $W$-2 grid points. We have systematically varied $H$ and the difference between the $A$- and $B$-surface interactions, $\xi \equiv (\varepsilon^0_{AM} - \varepsilon^0_{BM})/\nu kT$. We always used $\varepsilon^0_{AM} = 0$. Simulations were done until at least $P$ had leveled off to a constant value. However, to limit the computation time, needed to do a systematic analysis, we did not

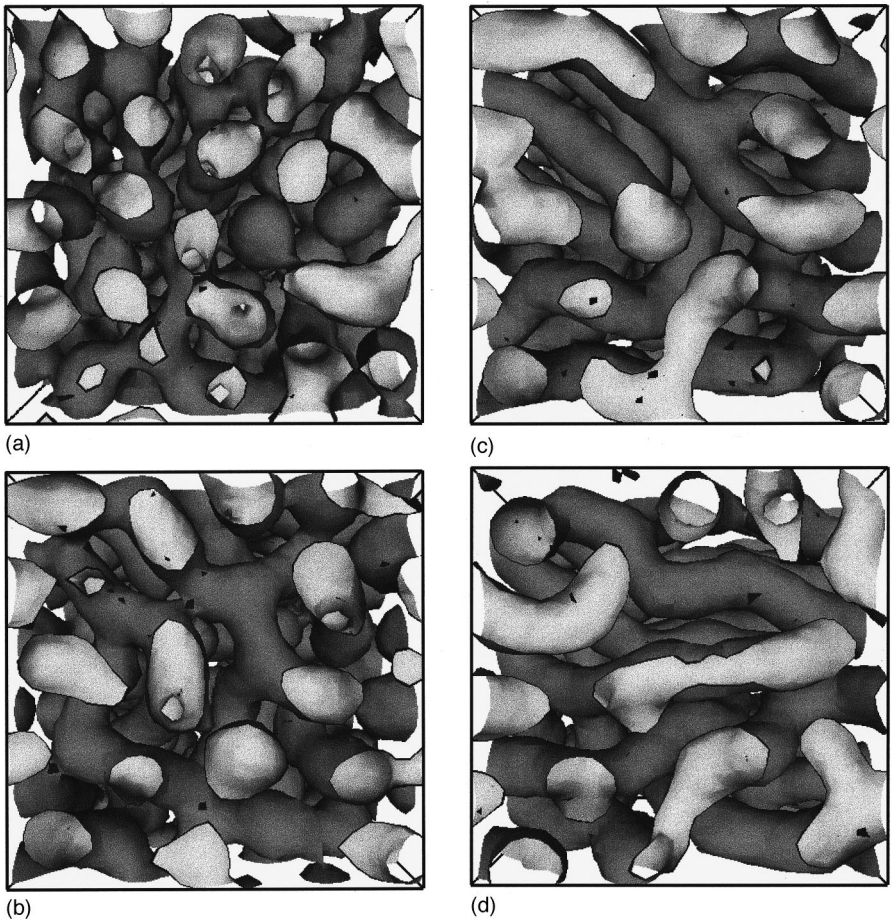


FIG. 2. The isodensity surfaces of the *A*-beads, $\phi_A = 0.33$, of a $32 \times 32 \times 32$ bulk system, (a) $y = 100$, (b) 200, (c) 1000, and (d) 10000.

always simulate until the morphology was defect free. The different phases were determined by visual assessment of the density profiles.

The results are listed in Table I. With this table we have constructed a phase diagram for the $A_3B_6$ model, Fig. 5. The black dots correspond with the calculations listed in Table I. The solid lines represent the proposed phase boundaries. Obviously, the obtained phase diagram is not complete and some of the proposed phase boundaries are supported by only two data points. In Fig. 6, we have plotted the isodensity surfaces of the *A*-beads ($\phi_A = 0.33$) of systems located at different points in the phase diagram. Various morphologies have been observed; parallel cylinders ($C_{\parallel}$), Figs. 6(a) and 6(b), perpendicular cylinders ($C_{\perp}$), Fig. 6(c), parallel lamellae ($L_{\parallel}$), Figs. 6(d) and 6(e), and parallel perforated lamellae, called cartenoid-lamellae,[47] ($CL_{\parallel}$), Fig. 6(f).

The phase diagram, Fig. 5, clearly shows that parallel morphologies are dominant around $\xi = 0$ and 1.75 ($C_{\parallel}$, $L_{\parallel}$, and $CL_{\parallel}$). This is caused by the preference of the surfaces for one of the polymer blocks. Figures 6(a) and 6(d) make clear that at $\xi = 0$ *A*-enriched layers are formed at the slit surfaces. At $\xi = 1.75$, *B*-rich layers develop adjacent to the surfaces, see Figs. 6(c) and 6(e). Due to the selective nature

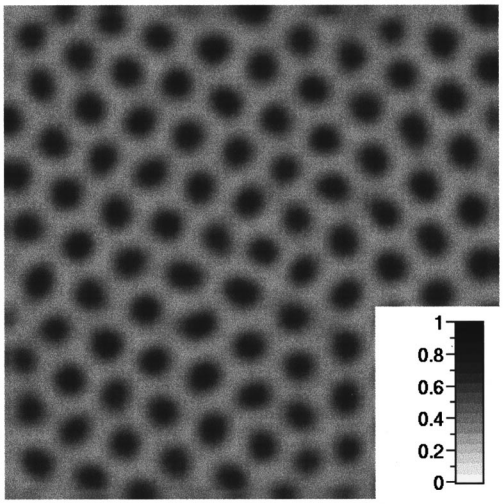


FIG. 3. The density profile of the *A* beads in a $64 \times 64 \times 1$ bulk system at $y = 4000$.

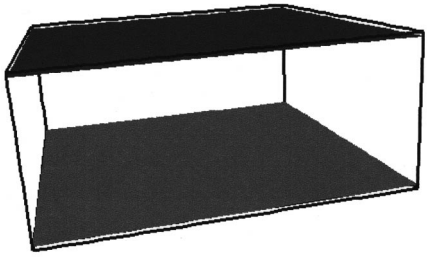

FIG. 4. The simulation box for slit calculations. The slit surfaces are placed at the top and bottom faces of the box. Periodic boundary conditions are applied at the other faces of the box.

TABLE I. An overview of all simulations, which have been done. Where $\xi \equiv (\varepsilon^0_{AM} - \varepsilon^0_{BM})/\nu kT$, $H$ is the slit width expressed in grid points, $l$ is the number of layers of $A$-rich domains excluding the boundary layers, and $y$ is the number of time steps of size $\Delta\tau$. The various observed morphologies are referred to with $C_\parallel$ (parallel cylinders), $C_\perp$ (perpendicular cylinders), $L_\parallel$ (parallel lamellae), and $CL_\parallel$ (cartenoid-lamellae).

| $\xi$ | $H$ | Phase | $l$ | $y \equiv \tau/\Delta\tau$ |
|---|---|---|---|---|
| 0 | 5 | $L_\parallel$ | - | 700 |
| | 6 | ,, | - | 300 |
| | 7 | ,, | - | 2000 |
| | 8 | $C_\perp$ | - | ,, |
| | 9 | ,, | - | ,, |
| | 10 | $C_\parallel$ | 1 | ,, |
| | 11 | ,, | 1 | ,, |
| | 12 | ,, | 1 | ,, |
| | 13 | ,, | 1 | ,, |
| | 14 | $C_\parallel + C_\perp$ | 1 | 6000 |
| | 15 | $C_\perp$ | - | 2000 |
| | 16 | $C_\parallel$ | 2 | ,, |
| 0.44 | 6 | $L_\parallel$ | - | 2000 |
| | 7 | $C_\perp$ | - | ,, |
| | 10 | ,, | - | ,, |
| | 11 | $C_\parallel$ | 1 | ,, |
| | 15 | $C_\perp$ | - | ,, |
| 0.73 | 12 | $C_\perp$ | - | 2000 |
| | 18 | | | ,, |
| 0.88 | 5 | $C_\perp$ | - | 4000 |
| | 6 | ,, | - | ,, |
| | 7 | ,, | - | 2000 |
| | 8 | ,, | - | ,, |
| | 9 | ,, | - | ,, |
| | 10 | ,, | - | ,, |
| | 11 | ,, | - | 4000 |
| | 12 | $C_\parallel$ | 2 | 2000 |
| | 13 | ,, | 2 | 6000 |
| | 14 | $C_\perp$ | - | 2000 |
| | 15 | ,, | - | ,, |
| | 16 | ,, | - | 2000 |
| | 17 | ,, | - | 4000 |
| | 18 | $C_\parallel$ | 3 | 2000 |
| | 20 | $C_\perp$ | - | ,, |
| | 22 | ,, | - | ,, |
| | 24 | $C_\parallel$ | 4 | 4000 |
| 1.32 | 6 | $CL_\parallel$ | 1 | 2000 |
| | 7 | $C_\parallel$ | 1 | ,, |
| | 8 | $C_\parallel + C_\perp$ | 1 | 600 |
| | 10 | $C_\perp$ | - | 2000 |
| | 11 | $C_\parallel$ | 2 | ,, |
| | 15 | $C_\perp$ | - | ,, |
| 1.75 | 5 | $L_\parallel$ | - | 2200 |
| | 6 | ,, | - | 2000 |
| | 7 | $CL_\parallel$ | 1 | ,, |
| | 8 | $C_\parallel$ | 1 | ,, |
| | 9 | $C_\perp$ | - | ,, |
| | 10 | $C_\parallel$ | 2 | ,, |
| | 11 | ,, | 2 | ,, |
| | 12 | ,, | 2 | ,, |
| | 13 | ,, | 2 | ,, |
| | 14 | ,, | 2 | ,, |
| | 15 | ,, | 2 | 8000 |
| | 16 | ,, | 3 | 2000 |

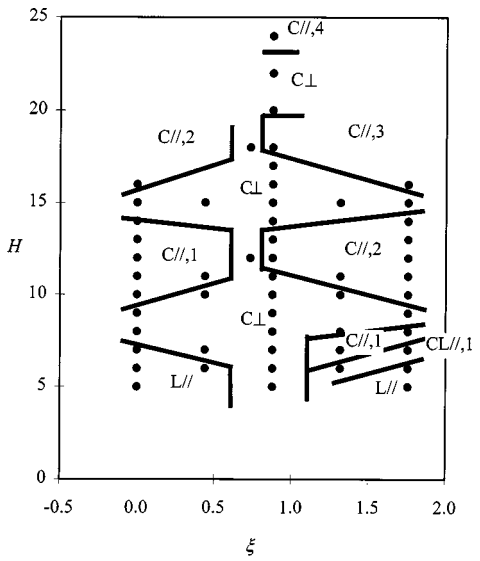


FIG. 5. The phase diagram of an $A_3B_6$ melt confined in a slit (film). The dots indicate where the simulations have been calculated. The thick solid lines are the proposed phase boundaries. The numbers added to the symbols are the $l$ values, listed in Table I.

of the slit surfaces, the polymer molecule has to orient itself in such a way that the $A/B$ interfaces and thus the microdomains have to align parallel with the slit surfaces, Fig. 7. It is interesting to notice that the slit surfaces behave as selective surfaces at $\xi = 0$, although both the $A$-surface and $B$-surface interactions were set to zero. Therefore, the preference for the $A$-blocks must have a purely entropic origin. Till now, the mechanism behind this entropic attraction is not understood.

Although, parallel morphologies are predicted for nearly every value of $H$ at $\xi \approx 0$ and 1.75, perpendicular cylinders, $C_\perp$, are formed at certain slit widths. Apparently, the domain–domain distance $D$ for the parallel cylindrical phase deviates to much from the bulk value at these widths and the surface–polymer interactions no longer compensate the increase of the free energy due to stretching or compression of the polymer chains. As a consequence, the cylinders adopt a perpendicular orientation in order reduce the stress on the polymer chains and $D \approx D_0$. This is confirmed by the fact that at both $\xi = 0$ and 1.75 the distance between two succeeding $C_\perp$-phases, $\Delta H$, is close to the closest distance between two layers of cylinders a bulk system, $\frac{1}{2} D_0 \sqrt{3} \approx 6$. This behavior has already been predicted for symmetric block copolymers confined in a slit with selective surfaces.[18,21] Parallel lamellae are formed at nearly all values of $H$, but at certain widths perpendicular lamellae are more stable.

The perpendicular cylindrical phase, $C_\perp$, dominates the phase diagram around $\xi = 0.75$. The energetic preference of the $B$-beads for the surface is balanced by the entropic preference of the $A$-beads. As a consequence, the surfaces act as nonselective surfaces. The elastic stress due to frustration of the domain–domain distance is not compensated by favorable surface–polymer interactions. Therefore, parallel cylinders are unstable compared to perpendicular cylinders for nearly every value of $H$. Again, the $A_3B_6$ polymer has the same behavior as a symmetric diblock copolymer.[18,19,21] In

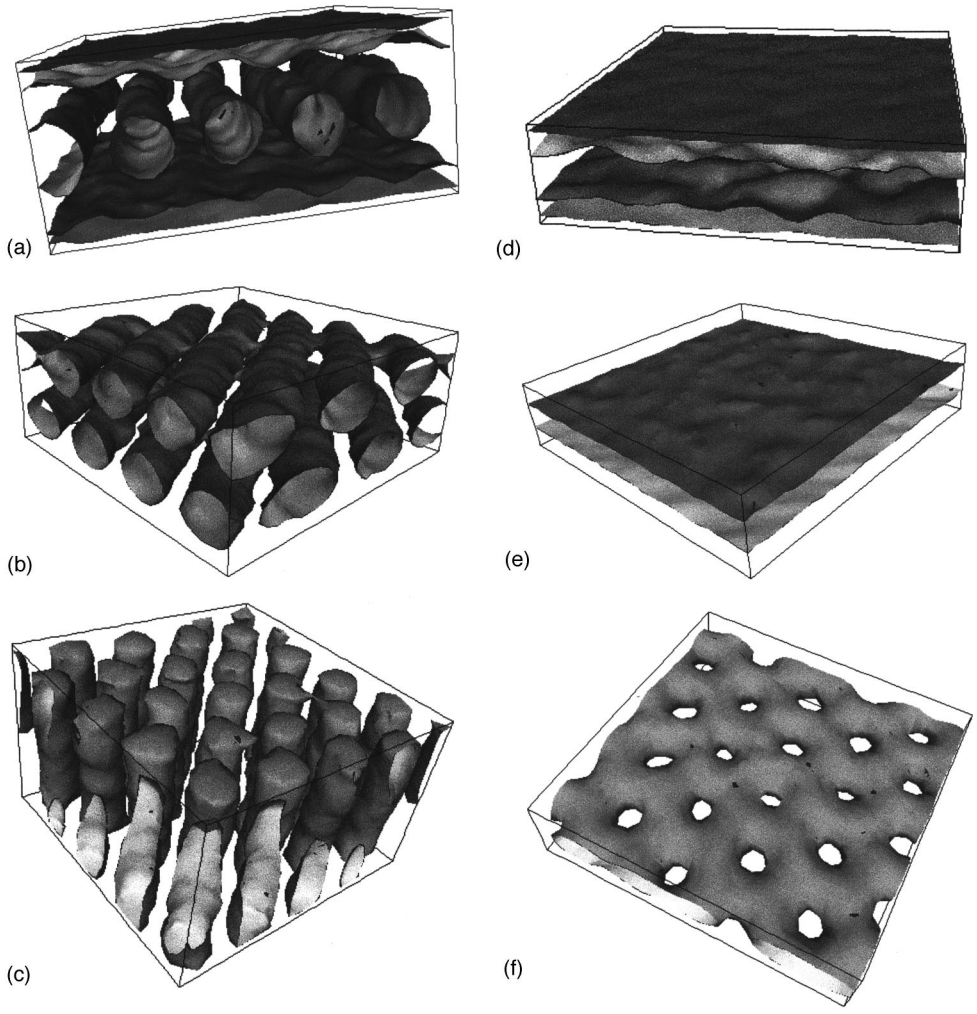


FIG. 6. The isodensity surfaces, $\phi_A = 0.33$, of various systems. The slit surfaces are always located at the top and bottom faces of the simulation box. Parallel cylindrical phases, $C_{\parallel}$: (a) $\xi = 0$ and $H = 13$ and (b) $\xi = 1.75$ and $H = 12$. Perpendicular cylindrical phase, $C_{\perp}$; (c) $\xi = 0.75$ and $H = 18$. Lamellar phases, $L_{\parallel}$: (d) $\xi = 0$ and $H = 7$ and (e) $\xi = 1.75$ and $H = 6$. Cartenoid-lamellar phase, $CL_{\parallel}$: (f) $\xi = 1.75$ and $H = 7$.

slits with selective surfaces lamellae dominate the phase diagram of a symmetric block copolymer. Perpendicular orientations of the lamellae are very stable in films with nonselective surface. The important difference between the $A_3B_6$ polymer and the symmetric block copolymer is the definition of a nonselective surface. This has the same origin as the fact that at $\xi = 0$ the *A*-block preferentially wets the surfaces.

Another interesting feature of the phase diagram is the existence of noncylindrical morphologies in slits with selective surfaces; lamellar ($L_{\parallel}$), Figs. 6(d) and 6(e), and cartenoid-lamellar ($CL_{\parallel}$) phases, Fig. 6(f). Lateral patterning is suppressed by the surface–polymer interactions, which are homogeneous parallel to the surface. Surface induced cylinder-lamellar transitions have already been predicted in the weak segregation limit (WSL).[32] It would be interesting to study the behavior of the phase diagram at $\xi < 0$ and $\xi > 1.75$. For reasons of time, we have limited ourselves to $\xi = [0,1.75]$. We expect that at larger slit widths, i.e., $H \approx 12$ or 17, the cylindrical phase will transfer in a cartenoid-lamellar or lamellar phase.

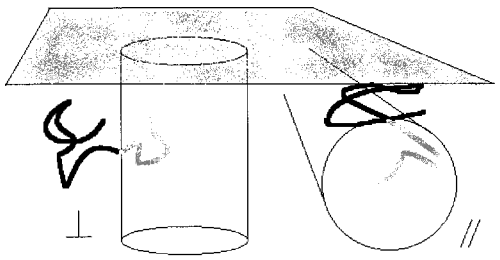


FIG. 7. The orientation of a diblock copolymer chain in a $C_{\parallel}$ (right) and $C_{\perp}$ (left) phases. When a cylinder orients parallel to the surface, the molecule is oriented perpendicular. A perpendicular orientation of the cylinder forces the molecule in a parallel orientation.

Finally, we want to compare the predicted phase diagram with experimental data, published in the literature. Two difficulties have to be faced. First, all experiments on asymmetric block copolymers are done with unconfined films and our calculations are done with a slit, which is comparable with a confined film. As a consequence, not all phases, predicted by the DDFT model, will be observed in the experiments. We will address this point in Sec. III D. Second, it is hard to locate the experimental systems accurately on the $\xi$-axis of our phase diagram.

A suitable experimental system for comparison with the $\xi > 1$ results, seems to be a PS–PB (polystyrene–polybutadiene) block copolymer with $f_S \approx 0.3$. In PS–PB films, the *B* block is preferentially adsorbed at the film interface. Unconfined films of this polymer have been studied in

detail with cross-sectional TEM.[28] Two different phases were observed; a $CL_{\parallel}$ structure in the thinnest part of the film and a $C_{\parallel}$ phases in the rest of the film. These two phases are predicted with the DDFT calculations. Even the order of the phases is predicted correctly. The DDFT predictions also agree with the experimental finding that a $CL_{\parallel}$ structure exists in films with a thickness, $H \approx 25-27$ nm, of the same order as the bulk domain–domain distance, $D_0 \approx 22$ nm. The DDFT model locates the $CL_{\parallel}$ phase at $H \approx 6-7$, which is of the same order as the predicted bulk domain–domain distance, $D_0 \approx 7$. It is interesting to compare the PS–PB and PS–PB–PS (Refs. 25, 30) studies. From AFM experiments[25] it had been concluded that the thinnest areas of the triblock copolymer films have a $C_{\perp}$ morphology. However, we think that what was called a $C_{\perp}$ phase is in fact a $CL_{\parallel}$ phase. With AFM it is hard to assign the domains to styrene or butadiene. This hinders the discrimination of the $C_{\perp}$ and $CL_{\parallel}$ phases in an AFM experiment, because both phases have a hexagonal structure viewed from the top.

The $\xi = 0$ side of the phase diagram can be compared with experimental data of unconfined films of PEP–PEE (PEP is polyethylene-propylene and PEE polyethylethylene),[24] $f_{\mathrm{PEP}} \approx 0.77$, and PS–PB,[22,28] $f_S \approx 0.7$. In both systems, the surfaces are preferentially wet by the smallest block, PEE and PB. In PEP–PEE films two structures have been observed; a $L_{\parallel}$ phase in the thinnest film and $C_{\parallel}$ phases at all other film thicknesses. Both phases are predicted by the DDFT model. As in the experiments, the DDFT predictions locate the $L_{\parallel}$ phase at $H \approx D_0$, Table I. In the PS–PB films a spherical or $C_{\perp}$ phase has been observed too.[28] This phase exist at film thicknesses between the $L_{\parallel}$ and the $C_{\parallel}$ phases, which agrees with our calculations.

At the end of this comparison with literature data, two remarks have to be made. First, experimental studies on films with nonselective surfaces have not been reported until now. Therefore, it is not possible to validate the region around $\xi = 0.75$ in the predicted phase diagram and the existence of the $C_{\perp}$ structures at high values of $H$ is still and open issue. In principle, it must be possible to do experiments on films with nonselective surfaces by coating the film substrate with a thin layer of a random copolymer, because this has already been done with films of symmetric block copolymers.[14,15] Second, we have predicted various $C_{\perp}$ phases at certain values of $H$ in slits with selective surfaces, but most of these phases are not observed in the experiments discussed above. We are convinced that this is a consequence of the difference between confined and unconfined films. As said before, a slit system is comparable with a confined film and the experiments on asymmetric block copolymer films were always done with unconfined films. In the next section, we will show that this is indeed the case. Direct evidence for these phases can only be obtained by experiments on confined films, which has already been done with symmetric diblock copolymers.[14]

### D. Unconfined films

In the preceding section, we discussed our slit calculations and compared the results with experimental data. Most of the perpendicular cylindrical phases were not found in the experimental studies. We have suggested that this is caused by the fact, that our slit calculations are comparable with confined films and all experiments were done with unconfined films. In Sec. II E we have already discussed that an unconfined film may avoid less favourable values of $H$ by the formation of terraces (separation in coexisting layers with different thicknesses). We have also explained that the terraces in unconfined films can be predicted with the free energy of confined films (in our case the slit). If our suggestion is true, the unfavorable thicknesses at, i.e., $\xi = 0$ should correspond with the predicted $C_{\perp}$ phases. In Fig. 8, we have plotted $\gamma \equiv h^2(F_{\mathrm{conf}} - F_{\mathrm{bulk}})/AkT$ as a function of $H$ for slits with $\xi = 0$. Note that $\gamma$ is in fact the surface tension. The solid dots are the calculated points and the dotted line represents the common tangent line. The negative sign of $\gamma$ is caused by the choice $\varepsilon^0_{AA} = \varepsilon^0_{BB} = 0$. It can be shown that nonzero values for these parameters give a width independent contribution to $\gamma$ and does not alter the density profiles.

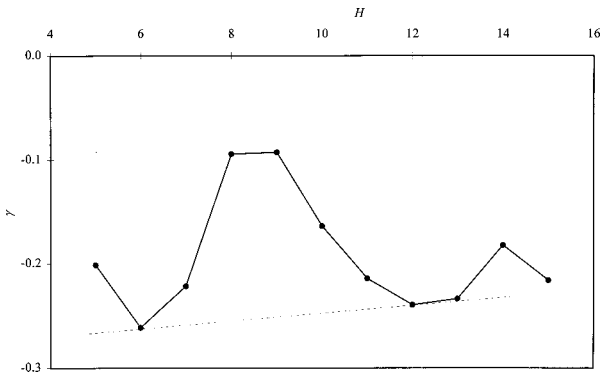


FIG. 8. The surface tension $\gamma$ as a function of the slit width $H$. The solid dots are the calculated points. The dashed line is the common tangent line, used to determine the stable film thicknesses in an unconfined film.

The maxima in the curve are located at $H = 9$ and 14, which corresponds with $C_{\perp}$ phases. The common tangent line makes clear that a film with an average thickness $H = 9$, will separate in a $L_{\parallel}$ and a $C_{\parallel}$ phase, Fig. 9(a). The same reasoning will hold for the behavior of an unconfined film with an average thickness $H = 14$. This film will separate into two coexisting $C_{\parallel}$ phases, Fig. 9(b). These predictions agree with the behavior of unconfined PEP–PEE films,[24] discussed in the preceding section. The formation of terraces of parallel oriented cylinders, $C_{\parallel}$ phases, has also been observed in PVP–PS films ($f_{\mathrm{PVP}} = 0.25$).[23]

### E. Dynamics in a slit

Beside information on the phase behavior of the $A_3B_6$ molecule in a slit, we also obtained a lot of data on the dynamics of microphase separation in a slit (confined thin film) by our simulations. In this section, we want to show that the slit has a strong influence on the ordering dynamics. However, a more extensive discussion is deferred to a following publication.

We have already observed in the $A_3B_6$ bulk calculations, section *B*, that the domain formation process consists of several processes with different time and length scales, e.g., the

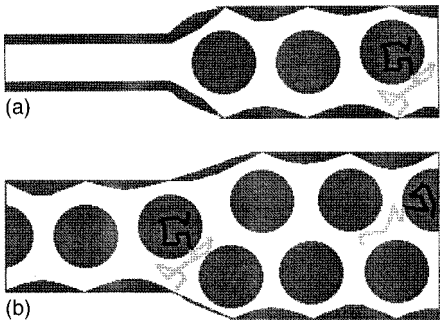


FIG. 9. A schematic picture of terrace formation in a $\xi=0$ film: (a) separation in coexisting $L_{\parallel}$ and $C_{\parallel}$ phases and (b) in two $C_{\parallel}$ phases.

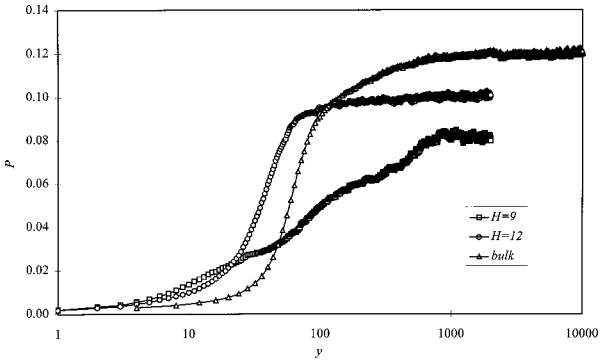


FIG. 10. The order parameter $P$ as a function of time $y$ for three different systems: $32\times32\times32$ bulk (△), slit $H=9$ and $\xi=0$() and slit $H=12$ and $\xi=0$(○).

formation a network of cylinders (short range order) from a homogeneous melt and the ordering of these cylinders in arrays (long range order).

An important effect of confinement on the ordering dynamics of $A_3B_6$ can be seen, when the iso-density surfaces of $A$ beads in a bulk system (Fig. 2) are compared with, i.e., the results of slit calculations shown in Fig. 6 and listed in Table I. Clearly, the formation of long range ordered structures is sped up by the slit. Whereas the time scale for long range ordering exceeds $y=10\,000$ in a bulk system, it is about $y=2000$ in most of the slit systems. This agrees with DDFT results on lamellae forming block copolymers.[38] The influence of the slit is at least twofold. First, it is known that external forces, like electric fields[48] and flow fields,[37] can reduce the time scales connected with long range ordering enormously. The influence of a slit on the ordering process can be thought of in terms of an external force. Second, in the direction perpendicular to the slit surfaces the system size is small compared to the bulk. Therefore, in a slit long range order has to be established in only two dimensions instead of three in the bulk.

The process of short range ordering, the formation of micro domains from a homogeneous melt, is also influenced by the slit. In Fig. 10 we have plotted the order parameter $P$ as a function of time for two slit systems ($\xi=0$), $H=9$ (squares) and $H=12$ (circles), together with the bulk system (triangles), discussed in Sec. B (Fig. 1). These curves already show that the influence of the slit on the demixing process of the $A$ and $B$ blocks is less universal as on the long range ordering. Initially, $y<20$, the demixing of the $A$ and $B$ beads is enhanced in both slit systems, compared to the bulk system. We have plotted the isodensity surfaces of the $A$ beads at $y=20(\phi_A=0.33)$ for both slit systems in Figs. 11(a) and 11(b). In both slits the $A$ and $B$ blocks are weakly segregated in layers parallel to the surfaces. This layering is induced by the surfaces, because the $A$ blocks are attracted for reasons already discussed in the preceding section. Large differences in the demixing behavior appear at $y>20$. For $H=12$ the order parameter rapidly increases to a semiplateau value at about $y=100$. At $y=100$ a 2D network of $A$-rich cylinders has developed parallel to the surface, Fig. 11(c). Above $y=100$ $P$ only slowly increases. The nodes in the network disappear and a parallel cylinders remain, which have already been shown in Fig. 6(a). Where the demixing in the $H=12$ system accelerates above $y=20$, the demixing in the $H=9$ system continues more gradually. Even the demixing of a bulk system takes place much faster. The amplitude of the initially developed density oscillations, producing parallel layers, does not grow further. The period of the density oscillation, which equals 4.5, deviates to much from the distance between two neighbouring layers of cylinders in a bulk system, $\frac{1}{2}D_0\sqrt{3}$, to form a stable parallel structure. Further segregation takes place in perpendicular oriented domains, Fig. 11(d). The rearrangement of the micro structure from a parallel to perpendicular structure is a slow process. This has already been predicted for lamellae forming systems with a Landau–Ginzburg-type of theory.[33]

It is likely that besides the slit width $H$ also the selectivity of the slit surfaces $\xi$ will have a strong influence on the process of short range ordering. A systematic analysis of the ordering process as a function of $\xi$ and $H$, as we have done for the static behavior in Sec. III C, deserves further attention.

## IV. CONCLUSIONS

A dynamic density functional theory has been used to study the microdomain formation in thin films of asymmetric block copolymers, $A_3B_6$. A thin film was represented as a slit with hard walls.

We have found that the microstructure of an $A_3B_6$ bulk system consists of $A$-rich cylinders embedded in a $B$-rich matrix. These cylindrical structure orders into a hexagonal pattern.

A systematic analysis of the influences of the film thickness and the surface–polymer interactions on the final morphology of $A_3B_6$ thin films has been carried out. We were able to construct a phase diagram. Various morphologies have been predicted: parallel cylinders ($C_{\parallel}$), perpendicular cylinders ($C_{\perp}$), parallel lamellae ($L_{\parallel}$), and cartenoid-lamellae ($CL_{\parallel}$).

Parallel morphologies are dominant in films with surfaces having a preference for one of the blocks of the copolymer (selective surfaces). Due to the surface induced orientation of the block copolymer, the microdomains have to arrange parallel to the surfaces. However, at certain thicknesses perpendicular cylinders were formed. At these thicknesses, the gain in energy due to favorable surface–polymer

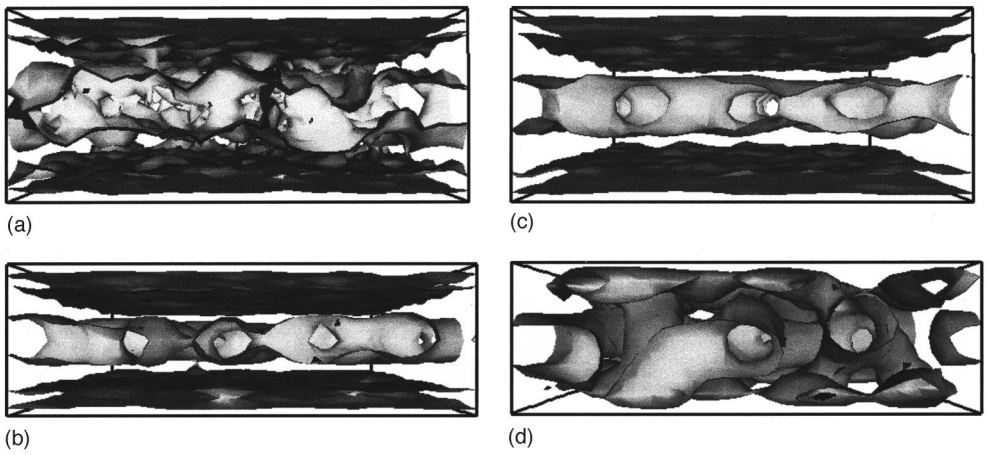


FIG. 11. The isodensity surfaces, $\phi_A = f_A \approx 0.33$, in slit systems with $\xi = 0$: (a) $y = 20$ and $H = 12$, (b) $y = 20$ and $H = 9$, (c) $y = 100$ and $H = 12$, and (d) $y = 100$ and $H = 9$.

interactions is no longer sufficient to counteract the free energy loss, due to the stretching or compression of polymer chains in parallel morphologies. A region where perpendicular cylinders were stable for nearly every film thickness, has been found too. In this region, neither the *A*- nor the *B*-block preferentially wets the film surfaces and the surfaces have an energetic preference for the largest block of the polymer, needed to balance the entropic preference for the shortest block. The mechanism behind this entropic preference is still not understood and deserves further attention. Generally, we can conclude that the orientation phenomena seem to be the same as in lamellae forming systems.

For the thinnest films transitions from cylindrical to noncylindrical structures, like lamellae and cartenoid-lamellae, have been predicted. These transitions occur when the preference of the film surfaces for one of the blocks increases. The strength of the surface–polymer interactions does not vary in de direction parallel to the surfaces. As a consequence, spatial variations in density fields in this direction are suppressed and the cylinder to lamellae or cylinder to cartenoid lamellae transitions are promoted. We expect that these transitions will also occur in thicker films when the polymer–surface interaction is high enough. This deserves further research in the future.

The predicted phase diagram agreed with the experimental data on cylinder-forming diblock copolymers. Therefore, we can conclude that the observed morphologies in thin films of *AB*-type asymmetric block copolymers are mainly governed by the film thickness and the surface–polymer interactions. For various reasons some of the predicted phases are not observed in experiments. First, the region of the phase diagram, where perpendicular cylinders are dominant, has not been accessed by experiments until now. To study this region of the phase diagram, random copolymers could be used to tune the surface–polymer interactions. Second, although perpendicular cylindrical phases are predicted at certain film thicknesses for films with selective surfaces, these phases are not observed in experiments. This difference is caused by the fact that the experiments have been carried out with unconfined films and our calculations are done with confined systems.

We have briefly studied the influence of the slit on the ordering dynamics. We have found that in a slit the process of long range ordering was enhanced compared to the bulk. The influence on the ordering a smaller length scales, the demixing of the blocks in separate domains, was less universal. A more systematic study has to be done.

## ACKNOWLEDGMENTS

This study has been carried out at the Shell Research and Technology Center in Amsterdam (SRTCA). We thank Wouter Koot (Shell) for his comments on this paper and Andrei Zvendilovsky and Hans Fraaije (University of Groningen) for the useful discussions. Support to this project was provided by the MesoDyn Project ESPRIT No. EP22685 of the European Community.

[1] F. S. Bates and G. H. Fredrickson, Annu. Rev. Phys. Chem. **41**, 525 (1990).
[2] G. H. Fredrickson and F. S. Bates, Annu. Rev. Mater. Sci. **26**, 501 (1996).
[3] M. W. Matsen, Curr. Opin. Colloid Interface Sci. **3**, 40 (1998).
[4] K. Binder, Adv. Polym. Sci. **138**, 1 (1999).
[5] S. H. Anastasiadis, T. P. Russell, S. K. Satija, and C. F. Majkrzak, Phys. Rev. Lett. **62**, 1852 (1989).
[6] G. Coulon, T. P. Russell, V. R. Deline, and P. F. Green, Macromolecules **22**, 2581 (1989).
[7] B. Collin, D. Chatenay, G. Coulon, D. Ausserre, and Y. Gallot, Macromolecules **25**, 1621 (1992).
[8] M. D. Forster, M. Sikka, N. Singh, F. S. Bates, S. K. Satija, and C. F. Majkrzak, J. Chem. Phys. **96**, 8605 (1992).
[9] A. M. Mayes, T. P. Russell, P. Bassereau, S. M. Baker, and G. S. Smith, Macromolecules **27**, 749 (1994).
[10] M. Sikka, N. Singh, A. Karim, F. S. Bates, S. K. Satija, and C. F. Majkrzak, Phys. Rev. Lett. **70**, 307 (1993).
[11] T. P. Russell, P. Lambooy, J. G. Barker, P. Callagher, S. K. Satija, G. J. Kellogg, and A. M. Mayes, Macromolecules **28**, 787 (1995).
[12] T. P. Russell, P. Lambooy, G. J. Kellogg, and A. M. Mayes, Physica B **213&214**, 22 (1995).
[13] N. Koneripalli, N. Singh, R. Levicky, F. S. Bates, P. D. Callagher, and S. K. Satija, Macromolecules **28**, 2897 (1995).
[14] G. J. Kellogg, D. G. Walton, A. M. Mayes, P. Lambooy, T. P. Russell, P. D. Callagher, and S. K. Satija, Phys. Rev. Lett. **14**, 2503 (1996).

[15] E. Huang, T. P. Russell, C. Harrison, P. M. Chaikin, R. A. Register, C. J. Hawker, and J. Mays, Macromolecules **31**, 7641 (1998).
[16] M. S. Turner, Phys. Rev. Lett. **69**, 1788 (1992).
[17] K. R. Shull, Macromolecules **25**, 2122 (1992).
[18] D. G. Walton, G. J. Kellogg, A. M. Mayes, P. Lambooy, and T. P. Russell, Macromolecules **27**, 6225 (1994).
[19] M. Kikuchi and K. Binder, J. Chem. Phys. **101**, 3367 (1994).
[20] G. Brown and A. Chakrabarti, J. Chem. Phys. **102**, 1440 (1995).
[21] M. W. Matsen, J. Chem. Phys. **106**, 7781 (1997).
[22] C. S. Henkee, E. L. Thomas, and L. J. Fetters, J. Mater. Sci. **23**, 1685 (1988).
[23] Y. Liu, W. Zhao, X. Zheng, A. King, A. Singh, M. H. Rafailovich, J. Sokolov, K. H. Dai, E. J. Kramer, S. A. Schwarz, O. Gebizlioglu, and S. K. Sinha, Macromolecules **27**, 4000 (1994).
[24] A. Karim, N. Singh, M. Sikka, F. S. Bates, W. D. Dozier, and G. P. Felcher, J. Chem. Phys. **100**, 1620 (1994).
[25] M. A. van Dijk and R. van den Berg, Macromolecules **28**, 6773 (1995).
[26] P. Mansky, P. Chaikin, and E. L. Thomas, J. Mater. Sci. **30**, 1987 (1995).
[27] P. Mansky, C. K. Harrison, P. M. Chaikin, R. A. Register, and N. Yao, Appl. Phys. Lett. **68**, 2586 (1996).
[28] L. H. Radzilowski, B. L. Carvalho, and E. L. Thomas, J. Polym. Sci., Part B: Polym. Phys. **34**, 3081 (1996).
[29] J. Hahm, W. A. Lopes, H. M. Jaeger, and S. J. Sibener, J. Chem. Phys. **109**, 10111 (1998).
[30] G. Kim and M. Libera, Macromolecules **31**, 2569 (1998).
[31] C. Harrison, M. Park, P. Chaikin, R. A. Register, D. H. Adamson, and N. Yao, Macromolecules **31**, 2185 (1998).
[32] M. S. Turner, M. Rubinstein, and C. M. Marques, Macromolecules **27**, 4986 (1994).
[33] G. Brown and A. Chakrabarti, J. Chem. Phys. **101**, 3310 (1994).
[34] R. D. Groot and T. J. Madden, J. Chem. Phys. **108**, 8713 (1998).
[35] J. G. E. M. Fraaije, B. A. C. van Vlimmeren, N. M. Maurits, M. Postma, O. A. Evers, C. Hoffmann, P. Altevogt, and G. Goldbeck-Wood, J. Chem. Phys. **106**, 4260 (1997).
[36] B. A. C. van Vlimmeren, N. M. Maurits, A. V. Zvelindovsky, G. J. A. Sevink, and J. G. E. M. Fraaije, Macromolecules **32**, 646 (1999).
[37] A. V. Zvendilovsky, G. J. A. Sevink, B. A. C. van Vlimmeren, N. M. Maurits, and J. G. E. M. Fraaije, Phys. Rev. E **57**, R4879 (1998).
[38] G. J. A. Sevink, A. V. Zvendilovsky, B. A. C. van Vlimmeren, N. M. Maurits, and J. G. E. M. Fraaije, J. Chem. Phys. **110**, 2250 (1999).
[39] N. M. Maurits, B. A. C. van Vlimmeren, and J. G. E. M. Fraaije, Phys. Rev. E **56**, 816 (1997).
[40] B. Schmittmann and R. K. P. Zia, *Statistical Mechanics of Driven Diffusive Systems* (Academic, London, 1995), p. 19.
[41] B. A. C. van Vlimmeren and J. G. E. M. Fraaije, Comput. Phys. Commun. **99**, 21 (1996).
[42] M. Doi and S. F. Edwards, *The Theory of Polymer Dynamics* (Clarendon, Oxford, 1986).
[43] E. Helfland, J. Chem. Phys. **62**, 999 (1975).
[44] N. M. Maurits, P. Altevogt, O. A. Evers, and J. G. E. M. Fraaije, Comput. Theor. Polym. Sci. **6**, 1 (1996).
[45] C. D. Han, J. Kim, and J. K. Kim, Macromolecules **22**, 383 (1989).
[46] J. D. Vavasour and M. D. Whitmore, Macromolecules **25**, 5477 (1992).
[47] E. L. Thomas, D. M. Anderson, C. S. Henkee, and D. Hoffman, Nature (London) **334**, 598 (1988).
[48] K. Amundson, E. Helfland, X. Quan, and S. D. Smith, Macromolecules **26**, 2698 (1993).